Confronting the fourth generation two-Higgs-doublet model with the phenomenology of heavy Higgs bosons

Sin Kyu Kang,[1] Zhuoni Qian,[2] Jeonghyeon Song,[3] and Yeo Woong Yoon[3]

[1]*School of Liberal Arts, Seoul National University of Science and Technology, Seoul 01811, Korea*
[2]*Center for Theoretical Physics of the Universe, Institute for Basic Science (IBS), Daejeon, 34126, Korea*
[3]*Department of Physics, Konkuk University, Seoul 05029, Korea*

A sequential fourth generation is known to be excluded because the nondecoupling contribution to κ_g, the Higgs coupling modifier with a gluon pair, is unacceptably large. Recently a new way to save the model was suggested in the type-II two-Higgs-doublet model: If the Yukawa couplings of down-type fermions have the wrong sign, the contributions from t' and b' to κ_g are canceled. We study the theoretical and experimental constraints on this model, focusing on the heavy Higgs bosons. We point out two constraining features. First, the exact wrong-sign limit does not allow alignment, which causes the perturbative unitarity for the scalar-scalar scattering to put upper bounds on the heavy Higgs boson masses like M_H, $M_A \lesssim$ 920 GeV and $M_{H^\pm} \lesssim 620$ GeV. Second, the Yukawa couplings of the fourth generation fermions to the heavy Higgs bosons are generically large, being proportional to the heavy fermion mass and, for the down-type fermions, to $\tan\beta$ as well. The gluon fusion production of H and A through the fourth generation quark loops becomes significant. We find that the current LHC data on $pp \to ZZ$ for H, along with the theoretical and indirect constraints, exclude the model at leading order.

I. INTRODUCTION

Our greatest hope for new physics (NP) beyond the standard model (SM) has not been fulfilled yet since the dedicated searches for new particles at the LHC found no new signals, and various precision data are consistent with the SM predictions. The usual strategy for a NP theory is to hide it in the decoupling limit: Very heavy new particles cannot be observed at the current 13 TeV LHC, nor do they significantly contribute to the precision data, including the Higgs signals. One important exception is a sequential fourth generation model where the new chiral fermions (t', b', ν' and τ') acquire their masses via the same Higgs mechanism. This model is motivated by the question of whether there exist only three fermion generations in the Universe [1–3]. The discovery of the SM-like Higgs boson with a mass of 125 GeV [4,5] excludes this model since the contributions of the heavy fourth generation quarks to the gluon fusion production of the Higgs boson do not decouple but saturate to a constant value which is unacceptably large.

Based on the observation that the NP contribution to the Higgs coupling modifier with a gluon pair, κ_g, is proportional to the sum of the Higgs coupling modifiers of t' and b', i.e., $(\kappa_{t'} + \kappa_{b'})$ when $M_{t'}$, $M_{b'} \gg m_h$, the authors of Ref. [6] found that the sequential fourth generation model can survive the Higgs precision constraint if the down-type quark Yukawa coupling has opposite sign to that of the up-type quark, i.e., $\kappa_{b'} = -\kappa_{t'}$. More interesting is that in the exact wrong-sign limit where all of the down-type fermions have opposite Higgs coupling to the up-type fermion, the new contributions to $\kappa_{\gamma\gamma}$ and $\kappa_{Z\gamma}$ also vanish. The wrong-sign Yukawa couplings for the down-type fermions cannot be realized in the SM with only one Higgs doublet [7]: The Higgs sector should be extended as in the two-Higgs-doublet model (2HDM) [8–12]. Reference [6] showed that the type-II 2HDM with a sequential fourth generation satisfies not only the Higgs signal strength measurements but also the oblique parameters ΔS and ΔT. Follow-up studies focused on top-quark dipole moments [13], dark matter [14], and lepton flavor changing in the Higgs boson decays [15].

Despite the appeal of the model in satisfying the Higgs precision constraint through such a simple remedy, this model has a potentially dangerous spot, the phenomenology of the heavy Higgs bosons. The 2HDM has five physical Higgs bosons, the light CP-even scalar h, the heavy CP-even scalar H, the CP-odd pseudoscalar A, and

two charged Higgs bosons $H^\pm$. With a sequential fourth generation, the Yukawa couplings of the fourth generation fermion F with all the Higgs bosons are proportional to the fermion mass M_F, which is naturally very large. In addition, the down-type fermion Yukawa couplings with H and A, $Y_{b'}^{H/A}$, are proportional to $\tan\beta$, while the up-type fermion couplings are inversely proportional to $\tan\beta$, where $\tan\beta$ is the ratio of two vacuum expectation values (VEVs) of two Higgs doublet fields. The cancellation of t' and b' contributions to the hgg coupling does not occur in the Hgg and Agg couplings. At the LHC, H and A can be copiously produced.

Another concern is from the exact wrong-sign limit, the key that allows the sequential fourth generation. It relates two mixing angles α and β through $\alpha + \beta = \pi/2$, where α is the mixing angle between h and H. Unless $\tan\beta$ becomes very large, the exact wrong-sign limit cannot approach the alignment limit of $\sin(\beta - \alpha) = 1$. Since too-large $\tan\beta$ breaks the perturbativity of $Y_{b'}^{H/A}$, the exact wrong-sign limit brings about a significant deviation from the alignment limit. One important consequence is the different dependence of the scalar quartic couplings on the heavy Higgs boson masses from the alignment limit. As will be shown, this difference has a strong impact on the perturbative unitarity of scalar-scalar scattering, the *upper* bounds on the heavy Higgs boson masses. The decoupling limit cannot be achieved along with the exact wrong-sign limit. The model does not have a safety zone. We need a comprehensive study on the phenomenology of the model, including the heavy Higgs bosons, which is our main purpose.

This paper is organized as follows. In Sec. II, we review the type-II 2HDM with a sequential fourth generation in the exact wrong-sign limit. The Higgs coupling modifiers in this model are compared with those in the alignment limit, with special focus on κ_V. Section III deals with the theoretical constraints on the scalar sector: the bounded-from-below potential, unitarity, perturbativity, and vacuum stability. Here we explicitly show that the dependence of λ_3 on M_H is very different from that in the alignment limit. In Sec. IV, we study the indirect constraints from the electroweak oblique parameters and the Higgs precision data. The observed κ_V restricts $\tan\beta$ significantly. Based on the narrowed parameter space from the theoretical and indirect constraints, we study the decay and production of H and A in Sec. V. Here we point out that above the $b'\bar{b}'$ threshold, the total decay widths of both H and A become wide like $\Gamma_{\rm tot}^{H/A} \sim M_{H/A}$. The ordinary analysis based on $\sigma \times \mathcal{B}$ does not work here. We suggest a method to probe this very broad resonance, not relying on the total event counting. The production cross sections of the gluon fusion of H and A are also studied. In Sec. VI, we consider direct search results for new particles at the LEP and LHC, $e^+e^- \to 4b$, 4τ, $2b2\tau$ and $pp \to \tau\tau$, ZZ, Zh. Two smoking-gun signals, Zh for A and ZZ for H, are elaborated, drawing a rather strong conclusion that this model at leading order is excluded by the combination of theoretical and experimental constraints. In Sec. VII, we summarize and conclude.

II. REVIEW OF THE 2HDM-SM4

We consider a 2HDM with a sequential fourth generation in the exact wrong-sign limit. The Higgs sector and the fermion sector are extended by introducing two complex $SU(2)_L$ Higgs doublet scalar fields, Φ_1 and Φ_2 [16], and a sequential fourth generation, respectively:

$$\Phi_i = \begin{pmatrix} w_i^+ \\ \frac{v_i + h_i + i\eta_i}{\sqrt{2}} \end{pmatrix}, \qquad \begin{pmatrix} t'_L \\ b'_L \end{pmatrix}, \qquad t'_R, \qquad b'_R,$$

$$\begin{pmatrix} \nu'_L \\ \tau'_L \end{pmatrix}, \qquad \nu'_R, \qquad \tau'_R, \tag{1}$$

where $i = 1, 2$, and $v_{1,2}$ is the nonzero VEV of $\Phi_{1,2}$. Note that the anomaly cancellation condition [17,18] requires the existence of the fourth generation leptons. When parametrizing $t_\beta = v_2/v_1$, one linear combination $H_1 = c_\beta \Phi_1 + s_\beta \Phi_2$ has nonzero VEV of $v = \sqrt{v_1^2 + v_2^2} = 246$ GeV, which generates the electroweak symmetry breaking. Its orthogonal combination $H_2 = -s_\beta \Phi_1 + c_\beta \Phi_2$ acquires zero VEV. For simplicity of notation, we take $s_x = \sin x$, $c_x = \cos x$, and $t_x = \tan x$.

In order to avoid flavor changing neutral currents (FCNC) at tree level, a discrete Z_2 symmetry is imposed, under which $\Phi_1 \to \Phi_1$ and $\Phi_2 \to -\Phi_2$ [19,20].[1] Then, the most general scalar potential with CP invariance and softly broken Z_2 symmetry is

$$V_\Phi = m_{11}^2 \Phi_1^\dagger \Phi_1 + m_{22}^2 \Phi_2^\dagger \Phi_2 - m_{12}^2(\Phi_1^\dagger \Phi_2 + {\rm H.c.})$$

$$+ \frac{1}{2}\lambda_1(\Phi_1^\dagger \Phi_1)^2 + \frac{1}{2}\lambda_2(\Phi_2^\dagger \Phi_2)^2 + \lambda_3(\Phi_1^\dagger \Phi_1)(\Phi_2^\dagger \Phi_2)$$

$$+ \lambda_4(\Phi_1^\dagger \Phi_2)(\Phi_2^\dagger \Phi_1) + \frac{1}{2}\lambda_5[(\Phi_1^\dagger \Phi_2)^2 + {\rm H.c.}]. \tag{2}$$

The CP invariance requires all of the parameters to be real. Note that the soft Z_2 symmetry breaking parameter m_{12}^2 can be negative.

There are five physical Higgs bosons, the light CP-even scalar h, the heavy CP-even scalar H, the CP-odd pseudoscalar A, and two charged Higgs bosons $H^\pm$. They are related with the weak eigenstates in Eq. (1) via

$$\begin{pmatrix} h_1 \\ h_2 \end{pmatrix} = \mathbb{R}(\alpha)\begin{pmatrix} H \\ h \end{pmatrix}, \qquad \begin{pmatrix} \eta_1 \\ \eta_2 \end{pmatrix} = \mathbb{R}(\beta)\begin{pmatrix} z^0 \\ A \end{pmatrix},$$

$$\begin{pmatrix} w_1^\pm \\ w_2^\pm \end{pmatrix} = \mathbb{R}(\alpha)\begin{pmatrix} w^\pm \\ H^\pm \end{pmatrix}, \tag{3}$$

---

[1]Recently, it was proposed that the addition of an Abelian gauge group can accommodate the absence of tree-level FCNC [21].

where z^0 and $w^{\pm}$ are the Goldstone bosons that will be eaten by the Z and W bosons, respectively. The rotation matrix $\mathbb{R}(\theta)$ is

$$\mathbb{R}(\theta) = \begin{pmatrix} c_\theta & -s_\theta \\ s_\theta & c_\theta \end{pmatrix}. \tag{4}$$

We consider the normal scenario where the observed Higgs boson is the lighter CP-even h, although the other scenario with $M_H = 125$ GeV is still allowed by the Higgs precision data [22,23].

The Yukawa couplings are different according to the Z_2 parity of the fermions. We fix $Q_L \rightarrow Q_L$ and $L_L \rightarrow L_L$ under Z_2 symmetry, where Q_L and L_L are the left-handed quark and lepton doublets, respectively. Then, each right-handed fermion field only couples to one scalar doublet field. There are four different ways to assign the Z_2 symmetry on the right-handed fermion fields, leading to four different types in the 2HDM: type-I, type-II, type-X, and type-Y. We parametrize the Yukawa interactions with the neutral Higgs bosons as

$$-\mathcal{L}_{\text{Yuk}} = \sum_f \frac{m_f}{v}(\kappa_f \bar{f} f h + \xi_f^H \bar{f} f H - i\xi_f^A \bar{f} \gamma_5 f A). \tag{5}$$

Note that κ_f is the Higgs coupling modifier, parametrizing the NP effects on the Higgs couplings:

$$\kappa_i = \frac{g_{iih}}{g_{iih}^{\text{SM}}} \equiv 1 + \delta\kappa_i. \tag{6}$$

While κ_f's are different according to the 2HDM type, κ_V and ξ_V ($V = W^{\pm}$, Z) have the common leading order expressions

$$\kappa_V = s_{\beta-\alpha}, \qquad \xi_V = c_{\beta-\alpha}. \tag{7}$$

Because the observed Higgs boson at a mass of 125 GeV is very SM-like, the so-called alignment limit [24] is usually adopted in the 2HDM, defined by

$$\alpha = \beta - \frac{\pi}{2} \quad (\text{alignment limit})$$

$$\rightarrow \kappa_u = \kappa_d = 1, \qquad \kappa_V = 1, \qquad \xi_V = 0, \tag{8}$$

where $u = t$, t', ν' and $d = b$, b', τ, τ'. With a sequential fourth generation, however, this alignment limit does not guarantee a SM-like Higgs boson because of the large contribution from the fourth generation fermions to the loop-induced couplings of the Higgs boson, especially to κ_g:

$$\kappa_g = \frac{\kappa_t A_{1/2}^h(\tau_t) + \sum_F \kappa_F A_{1/2}^h(\tau_F)}{A_{1/2}^h(\tau_t)}, \tag{9}$$

where $\tau_f = m_h^2/4m_f^2$, $F = t'$, b', and the expression for the loop function $A_{1/2}^h(\tau)$ is given in Ref. [25]. It is known that $A_{1/2}^h(\tau_f)$ approaches the value of $4/3$ when $m_f \gg m_h$. In the alignment limit ($\kappa_{t'} = \kappa_{b'} = 1$) with $M_F \gg m_h$, therefore, the value of κ_g approaches 3. We conclude that a sequential fourth generation in the SM or the aligned 2HDM is excluded by the Higgs precision data.

Based on the observation that $\delta\kappa_g$ is proportional to $(\kappa_{t'} + \kappa_{b'})$ for $M_F \gg m_h$ and the current LHC data cannot determine the sign of κ_b yet, the exact wrong-sign limit [6,11,26] is suggested, given by

$$\alpha = \frac{\pi}{2} - \beta \, (\text{exact wrong} - \text{sign limit})$$

$$\rightarrow \kappa_u = 1, \quad \kappa_d = -1, \quad \kappa_V = \frac{t_\beta^2 - 1}{t_\beta^2 + 1}, \quad \xi_V = \frac{2t_\beta}{t_\beta^2 + 1}. \tag{10}$$

The wrong-sign Yukawa couplings for the down-type fermions cannot be realized in the SM where there exists only one scalar doublet field: all of the Yukawa couplings can be set positive by chiral rotation. We need an additional Higgs doublet field, which can be minimally realized in the 2HDM. Among four types of the 2HDM, only type-II can accommodate the exact wrong-sign limit where both b' and τ' have opposite Yukawa couplings to t' and ν'. In what follows, 2HDM-SM4 denotes the type-II 2HDM with a sequential fourth generation in the exact wrong-sign limit.

A more surprising feature of the exact wrong-sign limit is that new contributions from the sequential fourth generation fermions to $\kappa_{\gamma\gamma}$ and $\kappa_{Z\gamma}$ are also suppressed in the heavy M_F limit [6]:

$$\delta\kappa_{\gamma\gamma} \propto \sum_{f=t',b',\tau'} Q_f^2 N_C^f \kappa_f = 0,$$

$$\delta\kappa_{Z\gamma} \propto \sum_{f=t',b',\tau'} Q_f(T_3^f)_L N_C^f \kappa_f = 0, \tag{11}$$

where Q_f is the electric charge of the fermion f, N_C^f is the color factor, and $(T_3^f)_L$ is the isospin projection of the left-handed f_L.

In the 2HDM, however, there exist other Higgs bosons, H, A, and $H^{\pm}$. The exact wrong-sign condition simplifies $\xi_{u,d}^{H,A}$, defined in Eq. (5), into

$$\xi_u^H = \xi_u^A = \frac{1}{t_\beta} \equiv \xi_u, \qquad \xi_d^H = \xi_d^A = t_\beta \equiv \xi_d. \tag{12}$$

An immediate concern is that the Yukawa couplings of b' and τ' with H and A, proportional to the heavy fermion masses, can be dangerously large, especially in the large t_β limit. Theoretical principles and collider experiments associated with H and A constrain the model significantly.

We now specify the model parameters in the 2HDM-SM4. In the scalar potential sector, there are seven free parameters of m_{12}^2, t_β, and $\lambda_{1,...,5}$, after applying the tadpole conditions for m_{11} and m_{22}. Equivalently, we can take the physical parameters of m_h, M_H, M_A, $M_{H^\pm}$, m^2, α and β, where $m^2 = m_{12}^2/(s_\beta c_\beta)$ is chosen because of its efficiency to show the invariance under the reparametrization in the space of the Lagrangian [27]. Since $m_h = 125$ GeV is known and the exact wrong-sign limit relates α and β as $\alpha + \beta = \pi/2$, there are five free parameters in the scalar sector. In the fourth generation fermion sector, only their masses are unknown because their gauge and Yukawa couplings are the same as the SM fermions. In summary, the 2HDM-SM4 has the following model parameters:

$$t_\beta, \quad m^2, \quad M_H, \quad M_A, \quad M_{H^\pm}, \quad M_{t'},$$
$$M_{b'}, \quad M_{\tau'}, \quad M_{\nu'}. \tag{13}$$

Some brief comments on the fourth generation fermion masses M_F and $M_{H^\pm}$ are in order here. For M_F, there are two kinds of constraints working in opposite ways, one from the unitarity and the other from direct searches. First, the perturbative unitarity for the fermion-fermion scattering sets the upper mass bound as $m_{q'} \lesssim 550$ GeV and $m_{\ell'} \lesssim 1.2$ TeV [28,29]. On the other hand, direct searches for t' and b' at the LHC set the lower bounds of $M_{t'} \gtrsim 680$ GeV, under the assumption that the produced t' and b' decay into a SM quark accompanied by a W or Z boson [30]. If the mixing between the SM quarks and the fourth generation quarks is extremely small like $V_{i4} \lesssim 10^{-7}$, however, no limits can be set [30]. The CDF Collaboration took the assumption of specific flavor-mixing rates and put the lower bound on $M_{t'}$, $M_{b'} \gtrsim 335$–385 GeV [31,32]. With general flavor mixing, the lower mass bounds were recalculated to be as low as 290 GeV [33,34]. The fourth generation leptons have weaker bounds as $m_{\tau'} > 100.8$ GeV and $m_{\nu'} > 41$ GeV [35]. The charged Higgs boson mass in a type-II 2HDM is most strongly constrained by the FCNC process $\bar{B} \to X_s\gamma$. The updated next-to-next-to-leading order SM prediction of $\mathcal{B}_{SM}(\bar{B} \to X_s\gamma)$ [36,37] and the recent Bell result [38] get closer, yielding $M_{H^\pm} > 570(440)$ GeV for $t_\beta \gtrsim 2$ at 95% (99%) C.L. For $t_\beta \lesssim 2$, the lower bound on $M_{H^\pm}$ increases significantly. Note that the fourth generation quarks do not affect the process $\bar{B} \to X_s\gamma$ under the assumption of $V_{4i} \lesssim 10^{-7}$.

III. THEORETICAL CONSTRAINTS ON THE SCALAR POTENTIAL

The quartic coupling constants in the scalar potential V_Φ can be rewritten in terms of the physical mass parameters, which are in the exact wrong-sign limit

$$\lambda_1 = \frac{1}{v^2}[t_\beta^2(M_H^2 - m^2) + m_h^2],$$

$$\lambda_2 = \frac{1}{v^2}\left[\frac{1}{t_\beta^2}(M_H^2 - m^2) + m_h^2\right],$$

$$\lambda_3 = \frac{1}{v^2}[-m^2 + M_H^2 - m_h^2 + 2M_{H^\pm}^2],$$

$$\lambda_4 = \frac{1}{v^2}[m^2 + M_A^2 - 2M_{H^\pm}^2],$$

$$\lambda_5 = \frac{1}{v^2}[m^2 - M_A^2]. \tag{14}$$

They are constrained by the following theoretical conditions:

(1) The scalar potential V_Φ should be bounded from below in any direction, requiring [39,40]

$$\lambda_1 > 0, \qquad \lambda_2 > 0, \qquad \lambda_3 > -\sqrt{\lambda_1\lambda_2},$$
$$\lambda_3 + \lambda_4 - |\lambda_5| > -\sqrt{\lambda_1\lambda_2}. \tag{15}$$

(2) The tree-level perturbative unitarity demands [41–43]

$$|a_{i,\pm}| \leq 1, \tag{16}$$

where $a_{i,\pm}$ ($i = 1, ..., 6$) are the eigenvalues of the T matrix for the S-wave amplitudes of the scalar-scalar scattering, given by

$$a_{1,\pm} = \frac{1}{32\pi}\left[3(\lambda_1+\lambda_2)\pm\sqrt{9(\lambda_1-\lambda_2)^2+4(2\lambda_3+\lambda_4)^2}\right],$$

$$a_{2,\pm} = \frac{1}{32\pi}\left[\lambda_1+\lambda_2\pm\sqrt{(\lambda_1-\lambda_2)^2+4\lambda_4^2}\right],$$

$$a_{3,\pm} = \frac{1}{32\pi}\left[\lambda_1+\lambda_2\pm\sqrt{(\lambda_1-\lambda_2)^2+4\lambda_5^2}\right], \tag{17}$$

$$a_{4,\pm} = \frac{1}{16\pi}(\lambda_3 + 2\lambda_4 \pm 3\lambda_5),$$

$$a_{5,\pm} = \frac{1}{16\pi}(\lambda_3 \pm \lambda_4),$$

$$a_{6,\pm} = \frac{1}{16\pi}(\lambda_3 \pm \lambda_5). \tag{18}$$

(3) The perturbativity of scalar quartic couplings requires

$$|\lambda_i| < 4\pi, \qquad i = 1, ..., 5. \tag{19}$$

(4) The vacuum of V_Φ should be global, which happens if and only if [44]

$$D = m_{12}^2(m_{11}^2 - k^2 m_{22}^2)(t_\beta - k) > 0, \tag{20}$$

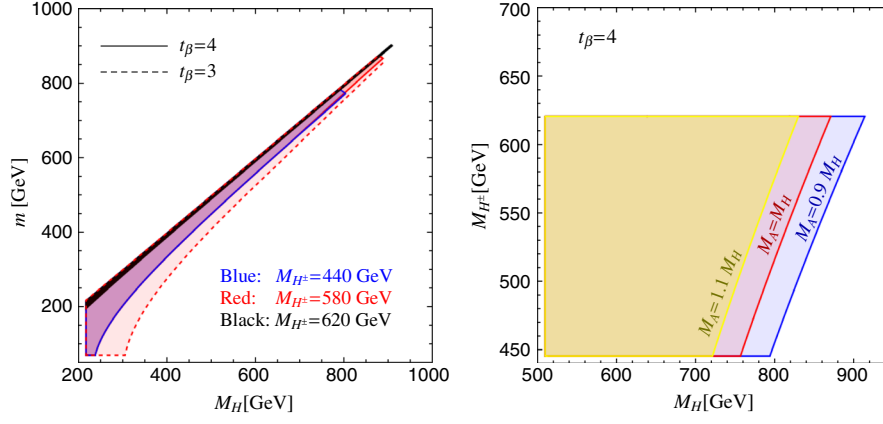where $k = (\lambda_1/\lambda_2)^{1/4}$.

FIG. 1. Left panel: Theoretically allowed parameter space of (M_H, m) for $t_\beta = 3, 4$, $M_{H^\pm} = 440, 580, 620$ GeV, and $M_A = 0.9M_H$. Right panel: Theoretically allowed parameter space of $(M_H, M_{H^\pm})$ for $t_\beta = 4$ and $M_A = (1 \pm 0.1)M_H$.

In the exact wrong-sign limit, the theoretical constraints are more difficult to satisfy than in the alignment limit. Crucial is λ_3, which shows different dependence on M_H:

$$\lambda_3 = \begin{cases} \frac{1}{v^2}[2M_{H^\pm}^2 + M_H^2 - m_h^2 - m^2] & \text{in the exact wrong-sign limit} \\ \frac{1}{v^2}[2M_{H^\pm}^2 - M_H^2 + m_h^2 - m^2] & \text{in the alignment limit.} \end{cases} \tag{21}$$

In both limits, λ_3 has the same dependence on $M_{H^\pm}^2$ but opposite signs for the M_H^2 terms. Since $M_{H^\pm}$ in a type-II 2HDM should be very heavy to explain the $b \to s\gamma$ result, heavy M_H in the exact wrong-sign limit should easily increase λ_3 above 4π. In the alignment limit, the negative M_H^2 contribution cancels the positive $M_{H^\pm}^2$ contribution to some extent since it is able to control the λ_3 value.

Figure 1 presents the theoretically allowed parameter space. In the left panel, we show the allowed parameter space[2] of (M_H, m) for $M_{H^\pm} = 440$ GeV and $t_\beta = 4$ (blue region), $M_{H^\pm} = 580$ GeV and $t_\beta = 3, 4$ (red region), and $M_{H^\pm} = 620$ GeV and $t_\beta = 4$ (black region). We also set $M_A = 0.9M_H$ in order to explain the oblique ΔT parameter. Two cases of $t_\beta = 3$ and $t_\beta = 4$ for the same $M_{H^\pm} = 580$ GeV show that small t_β allows more freedom for m, but it does not significantly change the allowed range for M_H. When t_β is very large, only a fine linear line along $M_H = m$ is allowed, irrespective of $M_{H^\pm}$. The most important result is that theoretical constraints put an *upper* bound on M_H, of which the $M_{H^\pm}$ dependence is small and the t_β dependence is negligible.

The charged Higgs boson mass is also bounded from above. In the right panel of Fig. 1, we show the theoretically allowed parameter space of $(M_H, M_{H^\pm})$ for $t_\beta = 4$. We consider three cases of $M_A = M_H$, $M_A = 1.1M_H$, and

$M_A = 0.9M_H$ to explain the oblique parameter ΔT. It can be seen that M_H cannot exceed about 920 GeV and $M_{H^\pm}$ should be smaller than 620 GeV. Since the t_β dependence on the upper bounds is negligible, as shown in the left panel of Fig. 1, the presence of the upper bounds on M_H, m, and $M_{H^\pm}$ is a generic feature of the 2HDM-SM4. We find that relaxing the degeneracy of M_H and M_A does not change the results much: The upper bound on M_H is about 945 GeV when $M_A \simeq 0.85M_H$. This result is unexpected. In the so-called normal mass hierarchy scenario where the observed 125-GeV scalar is the lighter h, it is usually expected that the theory can hide in the decoupling region. However, the exact wrong-sign limit does not allow decoupling of the theory. This is a unique feature of this model.

IV. INDIRECT CONSTRAINTS FROM OBLIQUE PARAMETERS AND HIGGS PRECISION DATA

In this section we narrow down the parameter space by applying the indirect constraints from the electroweak oblique parameters and the Higgs precision data.

A. Electroweak oblique parameters ΔS and ΔT

The oblique parameters ΔS and ΔT are affected by the sequential fourth generation fermions [28,45] as well as by new scalar bosons [46,47]. The current experimental data are consistent with the SM values, given by [35]

---

[2]Since only positive m^2 is allowed by the theoretical constraints, $m = \sqrt{m^2}$ is presented.

$$\Delta S = 0.05 \pm 0.10, \qquad \Delta T = 0.08 \pm 0.12, \quad (22)$$

where the parameter ΔT is more sensitive to new particles. It is well known that new contributions to ΔT are suppressed when the new particles running in the self-energy diagrams of gauge bosons have the same masses. We require that $M_{t'} \simeq M_{b'}$, $M_{\tau'} \simeq M_{\nu'}$, and two masses among M_H, M_A, and $M_{H^\pm}$ are degenerate. We also note that the contributions from H and A to the oblique parameter ΔT are negative [16], while those from the fourth generation fermions are positive [28,45,47]. Large mass splittings in the scalar and fourth generation fermion sectors are allowed if exquisite cancellation occurs. In this work, however, we do not consider the conspiracy between the new scalar sector and the new fermion sector in explaining the oblique parameters.

B. Higgs precision data

We take the combined analysis of ATLAS and CMS on the Higgs coupling modifier κ_i based on the LHC run 1 data, corresponding to integrated luminosities per experiment of 5 fb^{-1} at $\sqrt{s} = 7$ TeV and 20 fb^{-1} at $\sqrt{s} = 8$ TeV [48].[3] The analysis is based on a few assumptions, each of which constrains κ_i's differently. The 2HDM-SM4 model belongs to the category where new loop couplings beyond the SM (BSM) are allowed. The analysis result is that all κ_i's are consistent with the SM value. For the allowed values of κ_i's in this category, we refer the reader to Fig. 15 in Ref. [48].

The exact wrong-sign limit naturally explains the SM-like κ_t, $|\kappa_{b,\tau}|$, κ_g and κ_γ. One minor concern is $|\kappa_b|$, of which the maximum value at 2σ level is about 5% smaller than 1. Since a small deviation from the exact wrong-sign limit can easily accommodate this result, we stick to the exact wrong-sign limit as our reference point. On the other hand, κ_V can significantly deviate from 1. In Fig. 2, we show κ_V and ξ_V as a function of t_β. The observed κ_V requires very large t_β: If $\kappa_V = 0.98$, we need $t_\beta \approx 9.95$. However, too-large t_β violates the perturbativity of the Yukawa couplings of b' and τ' with H and A, $Y_{b',\tau'}^{H/A} = t_\beta M_{b',\tau'}/v$. If $\kappa_V = 0.98$ and $M_{b'} = 340$ GeV, e.g., we have $Y_{b'}^H = 13.8$. In summary, there is tension on the value of t_β: The observed κ_V pushes t_β upward; the perturbativity of the $Hb'\bar{b}'$ coupling presses t_β downward.

In Fig. 3, we summarize the constraints from the oblique parameter ΔT at 2σ level, the Higgs coupling modifier κ_V at 2σ level, and the perturbativity of $Y_{b'}^{H/A}$. Here $\Delta M_{DU} = M_{b'} - M_{t'} = M_{\tau'} - M_{\nu'}$ and $M_U (= M_{t'} = M_{\nu'})$ is fixed to be 300 GeV. The observed κ_V allows $t_\beta \gtrsim 3$, while the
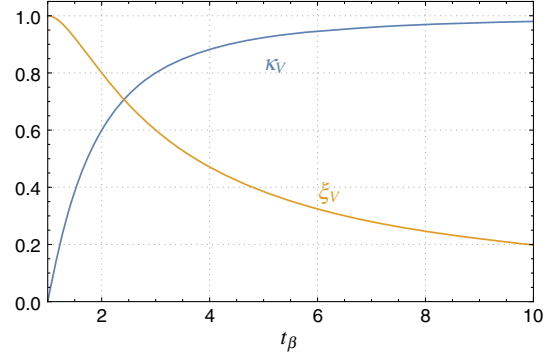
FIG. 2. κ_V and ξ_V as a function of t_β.

perturbativity of $Y_{b',\tau'}^{H/A}$ requires $t_\beta \lesssim 8$. The oblique parameter ΔT demands that the mass of an up-type fourth generation fermion be similar to that of the corresponding down-type fermion as $\Delta M/M \lesssim 20\%$.

In addition, the experimental result on exotic Higgs decay $\mathcal{B}_{BSM}^h \leq 0.34$ [48] has an important implication on the mass of the pseudoscalar A. In the 2HDM, M_A is a free parameter, so A can be light enough to kinematically allow $h \to AA$. The observed oblique parameter ΔT can be explained by the mass degeneracy $M_H \simeq M_{H^\pm}$. When writing $\mathcal{L} \supset \lambda_{hAA} AAh/2$, the partial decay rate is

$$\Gamma(h \to AA) = \frac{1}{32\pi m_h} \lambda_{hAA}^2 \sqrt{1 - \frac{4M_A^2}{m_h^2}}. \quad (23)$$

In the general 2HDM, λ_{hAA} is unknown for the given m_h and M_A because of an additional free parameter m^2. In the
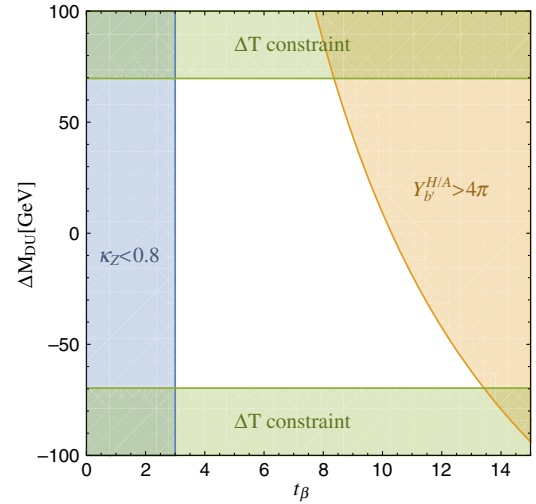

FIG. 3. The excluded regions of $(t_\beta, \Delta M_{DU})$ by the observed Higgs coupling modifier κ_V at 2σ level, the oblique parameter ΔT at 2σ level, and the perturbativity of $Y_{b'}^{H/A}$. Here $\Delta M_{DU} = M_{b'} - M_{t'} = M_{\tau'} - M_{\nu'}$ for the fixed $M_U = 300$ GeV. For the oblique ΔT parameter, we set $M_H = M_A = M_{H^\pm} = 600$ GeV.

exact wrong-sign limit ($\alpha + \beta = \pi/2$), however, the m^2 term is proportional to $c_{\beta+\alpha}$ and thus vanishes. The value of λ_{hAA} is determined by t_β and M_A as

$$\lambda_{hAA} = \frac{c_{2\beta}}{v}[2M_A^2 - m_h^2]. \tag{24}$$

The observed $\mathcal{B}_{\mathrm{BSM}}^h \leq 0.34$ is translated into $\Gamma(h \to AA) \lesssim \Gamma_{\mathrm{tot}}^{h,\mathrm{SM}}/2$, which can be satisfied when $0.9 \lesssim t_\beta \lesssim 1.1$ ($0.62 \lesssim t_\beta \lesssim 1.60$) for $M_A \ll m_h$ ($M_A = 62\,\mathrm{GeV}$). This small t_β region is excluded by the observed κ_V (see Fig. 2). In summary, a light pseudoscalar boson with $M_A \lesssim m_h/2$ in the 2HDM-SM4 is excluded by the observed $\mathcal{B}_{\mathrm{BSM}}^h$.

V. DECAY AND PRODUCTION OF H AND A

A. Decays

In this section, we discuss the decay and production of neutral heavy Higgs bosons, H and A. Considering the theoretical and direct search bounds on M_F, the perturbative unitarity of the scalar-scalar scattering, and the $b \to s\gamma$ constraint altogether, we take the following benchmark scenario:

$$m = M_H, \qquad M_A \approx M_H, \qquad M_{H^\pm} = 580\ \mathrm{GeV},$$

$$M_{t'} = 300\ \mathrm{GeV}, \qquad M_{b'} = 340\ \mathrm{GeV},$$

$$M_{\nu'} = 430\ \mathrm{GeV}, \qquad M_{\tau'} = 380\ \mathrm{GeV}. \tag{25}$$

Kinematically, the decays of $H \to AA$ and $H \to H^+H^-$ are prohibited. Note that the decays of $H \to W^\pm H^\mp$ and $A \to Zh$ are possible through the interaction Lagrangian of

$$\mathcal{L} \supset \frac{g_Z}{2}c_{\beta-\alpha}Z_\mu h\overleftrightarrow{\partial^\mu}A + i\frac{g}{2}s_{\beta-\alpha}[W_\mu H\overleftrightarrow{\partial^\mu}H^- + \mathrm{H.c.}], \tag{26}$$

where $g_Z = g/c_{\theta_W}$, θ_W is the weak mixing angle, and $\phi\overleftrightarrow{\partial^\mu}\eta = \phi\partial^\mu\eta - (\partial^\mu\phi)\eta$.

In Fig. 4, we show the branching ratios of H as a function of M_H for $t_\beta = 4$ and $m = M_H$. Before the WW threshold,
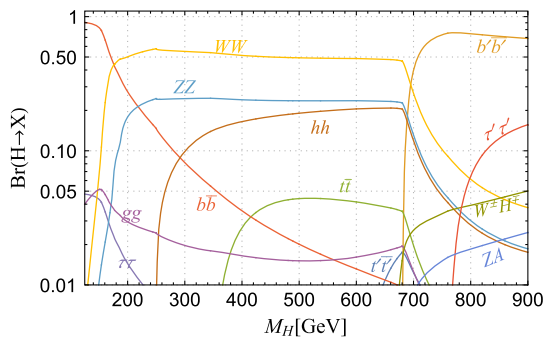
the dominant decay mode of H is into $b\bar{b}$, followed by $\tau\tau$ and gg modes because of the t_β enhancement in $Y_{b,\tau}^H$. After the WW/ZZ threshold, nonzero $\xi_V = c_{\beta-\alpha}$ ($c_{\beta-\alpha} \approx 0.47$ for $t_\beta = 4$) yields dominant decay of H into WW and ZZ because of the longitudinal polarization enhancement in the heavy scalar decay into a massive gauge boson pair [51].

For $M_H > 2m_h$, the decay of $H \to hh$ also becomes important. The triple Higgs coupling λ_{Hhh} in the exact wrong-sign limit is

$$\lambda_{Hhh} = \frac{c_{\beta-\alpha}}{v}\left(m^2 - \frac{1}{2}M_H^2 - m_h^2\right). \tag{27}$$

With the sizable $c_{\beta-\alpha}$ and the condition of $m \simeq M_H$ from the theoretical constraints shown in Fig. 1, the branching ratio of $H \to hh$ is substantial. Above the $t\bar{t}$ threshold, the $H \to t\bar{t}$ mode turns on, but not dominantly because the $Ht\bar{t}$ coupling is inversely proportional to t_β. For the same reason, the $H \to t'\bar{t}'$ mode is also minor even after the $t'\bar{t}'$ threshold. After the $b'\bar{b}'$ and $\tau'\tau'$ threshold, $H \to b'\bar{b}'$ is dominant and $H \to \tau'\tau'$ is the second dominant. The third dominant decay channel is into $H \to W^\pm H^\mp$, which always remains important because its vertex is proportional to $s_{\beta-\alpha}$ [see Eq. (26)].

The branching ratios of the CP-odd Higgs boson A as a function of M_A are shown in Fig. 5. We take the benchmark scenario in Eq. (25). Because of the CP-odd nature, A does not decay into WW, ZZ, or hh, but it does decay into Zh since the AZh vertex is proportional to non-negligible $c_{\beta-\alpha}$. Before the Zh threshold, the $b\bar{b}$ mode is dominant: The $Ab\bar{b}$ coupling also has t_β enhancement. The second dominant decay mode into gg has a much larger branching ratio than the $\tau\tau$ mode, unlike the case of H. This is because of the larger gg loop function for the CP-odd scalar than that for the CP-even scalar. When $m_Z + m_h < M_A < 2M_{b'}$, the decay of $A \to Zh$ is dominant, contrary to the alignment limit. In this mass range, the decay into gg is still important. We expect a sizable cross section of gluon fusion production of A. The branching ratios of the $t\bar{t}$ and $t'\bar{t}'$ modes are
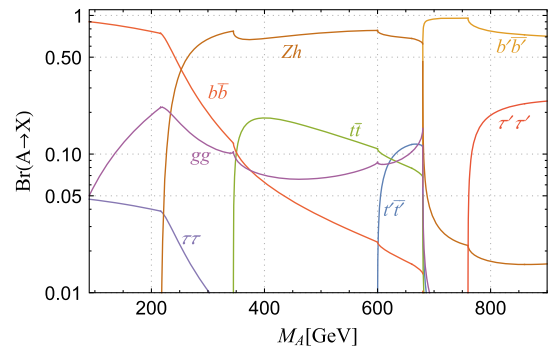

FIG. 4. The branching ratios of H as a function of M_H for $t_\beta = 4$. We set $M_{t'} = 300$ GeV, $M_{b'} = 340$ GeV, $M_{\nu'} = 430$ GeV, $M_{\tau'} = 380$ GeV, $m = M_H$, and $M_A = M_{H^\pm} = 580$ GeV.

FIG. 5. The branching ratios of A as a function of M_A for $t_\beta = 4$. We set $M_{t'} = 300$ GeV, $M_{b'} = 340$ GeV, $M_{\nu'} = 430$ GeV, $M_{\tau'} = 380$ GeV, and $m = M_H = M_{H^\pm} = 580$ GeV.

not as large as that of the Zh mode because both $At\bar{t}$ and $At'\bar{t}'$ couplings are inversely proportional to t_β. After the $b'\bar{b}'$ and $\tau'\tau'$ threshold, A decays into $b'\bar{b}'$ dominantly, followed by the $\tau'\tau'$ mode. The next dominant mode is into Zh with $\mathcal{B}(A \to Zh) \sim \mathcal{O}(1)\%$.

In Fig. 6, we show the total decay widths of H and A as a function of M_H and M_A for $t_\beta = 3$ and $t_\beta = 4$ in the benchmark scenario. For both H and A, $\Gamma_{\rm tot}$ increases rapidly with its mass, especially above the $b'\bar{b}'$ threshold. The dependence of $\Gamma_{\rm tot}^{H/A}$ on t_β is interesting. Before the $b'\bar{b}'$ threshold, the larger t_β is, the smaller the total decay width is. This behavior is due to the fact that the major decay modes before the $b'\bar{b}'$ threshold, $H \to WW/ZZ$ and $A \to Zh$, have partial decay rates that are all proportional to ξ_V^2, which decreases with increasing t_β (see Fig. 2). After the $b'\bar{b}'$ threshold, on the other hand, the dominant decay rate $\Gamma(H/A \to b'\bar{b}')$ is proportional to t_β^2.

Another crucial question related to $\Gamma_{\rm tot}$ is whether H and A can be probed as a narrow resonance so that the number of new events is proportional to the production cross section times the branching ratio. For reference, the LHC criteria as a narrow resonance is $\Gamma/M \le 1\%$ in the $\gamma\gamma$ channel [52,53], $\Gamma/M \le 0.5\%$ in the ZZ channel [49,54], and $\Gamma/M \le 15\%$ in the dijet channel [55]. When $t_\beta = 4$, e.g., heavy Higgs bosons like $M_H \gtrsim 350$ GeV and $M_A \gtrsim 300$ GeV do not belong to the narrow width category, which requires going beyond $\sigma \times \mathcal{B}$. Particularly above the $b'\bar{b}'$ threshold, both $\Gamma_{\rm tot}^H$ and $\Gamma_{\rm tot}^A$ are large like $\Gamma_{\rm tot} \sim M_H$. It is almost impossible to observe a mass peak in this mass region. We need a new strategy.

In order to deal with the very large width case, such as $\Gamma_{\rm tot}^{H/A} \sim M_{H/A}$, two points should be considered. First, we need a full calculation of $\sigma(pp \to ij)$ including the SM continuum background in order not to miss the significant interference. The second point is that new events spread out over multiple m_{ij} bins, not only to the bin of $m_{ij} = M$.
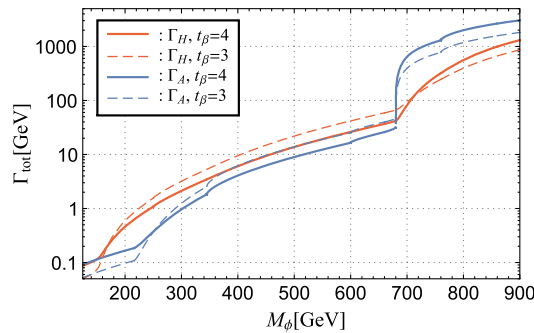
Without the possibility of observing a mass peak, we may rely on counting total events, which requires a very good understanding of the background. Or we can utilize the results of the usual analysis of the resonance searches for the excess in the invariant mass bins, which takes the following steps: (i) Events are collected in a specific m_{ij} bin; (ii) the number of events in the bin is compared with that of the expected background; (iii) no excess leads to the upper bounds on $\sigma \times \mathcal{B}(X \to ij)$ for a possible new particle with mass m_{ij}. Since multiple m_{ij} bins are affected by a single new particle when $\Gamma \sim M$, we need to calculate the excess of each m_{ij} bin nearby M and compare with the upper bounds on $\sigma \times \mathcal{B}(A \to Zh)$ for the corresponding bin. The size of each m_{ij} bin, ΔM, depends on the experimental analysis. Since our $d\sigma^{\rm NP}$ already includes the SM contributions, the excess over the SM backgrounds corresponds to the difference between the full $d\sigma^{\rm NP}$ and $d\sigma^{\rm SM}$. In order to compare with the excess in the $m_{ij} \in [M, M + \Delta M]$ bin, therefore, we calculate the partially integrated cross section $\Delta\sigma^{\rm NP}$ given by

$$\Delta\sigma^{\rm NP} = \int_M^{M+\Delta M} dm_{ij} \left[\frac{d\sigma^{\rm NP}(gg \to ij)}{dm_{ij}} - \frac{d\sigma^{\rm SM}(gg \to ij)}{dm_{ij}} \right].$$
(28)

We use this method when constraining very heavy A and H in the Zh and ZZ final states, respectively.

B. Production

We study the production of H and A. The production cross section of H/A with a small width is [56]

$$\sigma(pp \to H/A) = \frac{1}{sM_{H/A}} \sum_{\mathfrak{p}} C_{\mathfrak{p}\mathfrak{p}} \Gamma(H/A \to \mathfrak{p}\mathfrak{p}), \quad (29)$$

where $\mathfrak{p}$ is a parton in a proton and $C_{\mathfrak{p}\mathfrak{p}}$ is the $\mathfrak{p}\mathfrak{p}$ dimensionless partonic integral. Because $C_{b\bar{b}}/C_{gg} \sim 0.01$

FIG. 6. Total decay width of H and A as a function of their masses for two t_β cases, $t_\beta = 3$ and $t_\beta = 4$. We set $m = M_H$, $M_{t'} = 300$ GeV, $M_{b'} = 340$ GeV, $M_{\nu'} = 430$ GeV, and $M_{\tau'} = 380$ GeV, and do not include the decays of $H \to H^+ H^-$ and $H \to AA$.
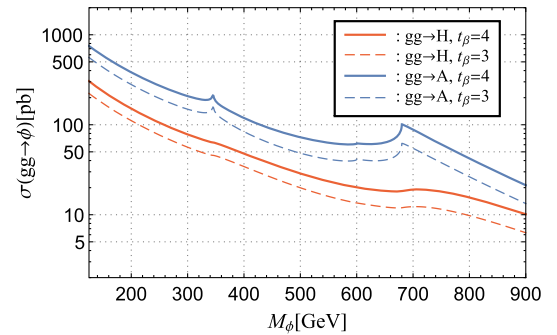
FIG. 7. The gluon fusion production cross sections of H and A as functions of M_H and M_A at the 13-TeV LHC for $t_\beta = 3$ and $t_\beta = 4$. We apply the NNLO K factor to the heavy Higgs resonance production by using the HIGLU package [57].

at the 13-TeV LHC and moderate $t_\beta \in [3, 8]$ implies not-too-large $Hb\bar{b}$ and $Ab\bar{b}$ couplings, we consider only the gluon fusion production. Figure 7 presents the gluon fusion production cross sections of H and A at the 13-TeV LHC as a function of M_H and M_A, respectively. We consider $t_\beta = 3$ and $t_\beta = 4$, and include the NNLO K factor by using the HIGLU package [57]. In the whole mass range, the production cross section is large: For M_H, $M_A = 600$ GeV, e.g., $\sigma(pp \rightarrow H/A) \sim \mathcal{O}(10)$ pb. The pseudoscalar A has a larger cross section than H because of the larger loop function for gg. As t_β increases, $\sigma(gg \rightarrow H/A)$ increases because the contribution from the b' quark in the loop is enhanced. For the CP-odd A, the threshold effects at $M_A = 2m_t$ and $M_A = 2M_{b'}$ are more prominent due to the cusp structure of the real part of the gg form factor $A^A_{1/2}(\tau)$ [58]. We caution the reader that the production cross section in Eq. (29) for $M_{H/A} \gtrsim 2M_{b'}$ gives just a rough estimation. When $\Gamma_{\text{tot}} \sim M_{H/A}$, the production of H/A itself is not meaningful. We need to set the final states ij and to perform the full calculation of $\sigma(pp \rightarrow ij)$, including the SM continuum background, because the interference effects crucially depend on the final state.

VI. CONSTRAINTS FROM DIRECT SEARCHES

In this section, we study the constraints from the direct searches for neutral scalar bosons at high energy colliders. The allowed region for the charged Higgs boson mass, $570 \lesssim M_{H^\pm} \lesssim 620$ GeV, is very difficult to probe because of the extremely small production rate of $H^\pm$ [59]. Our main target channels are summarized in Table I. Brief comments on $\gamma\gamma$, $\mu^+\mu^-$, and $b\bar{b}$ modes are in order here. Although the very clean $\gamma\gamma$ mode is searched for from $m_{\gamma\gamma} = 65(70)$ GeV by the ATLAS (CMS) experiments [60,61], it does not constrain the model since the branching ratio is very small: $\mathcal{B}(A \rightarrow \gamma\gamma) \sim \mathcal{O}(10^{-5})$ for $M_A = 65$ GeV. The data in the $\mu^+\mu^-$ channel [62] are also insufficient because of the extremely small $\mathcal{B}(H/A \rightarrow \mu^+\mu^-) \lesssim \mathcal{O}(10^{-4})$. The $b\bar{b}$ mode constrains a NP model only in the heavy mass range of $m_{b\bar{b}} \geq 800$ GeV [63] due to the huge QCD background, where both $\mathcal{B}(H \rightarrow b\bar{b})$ and $\mathcal{B}(A \rightarrow b\bar{b})$ are extremely small because of the dominant decays into $b'\bar{b}'$.

A. Constraints from direct searches on A

A meaningful constraint is from the neutral Higgs boson searches at the LEP through $e^+e^- \rightarrow H_i H_j$ ($H_{i,j} = h, H, A$) in the framework of the minimal supersymmetric standard model [64]. The analysis was based on four different decay channels of $4b$, $2b2\tau$, and 4τ. Since the searches span center-of-mass energies from 91 GeV to 209 GeV, the heavy CP-even H cannot be produced kinematically. The CP-odd scalar boson A is produced in association with h, mediated by the Z boson. With the observed Higgs boson mass of 125 GeV, the LEP result excludes $M_A \lesssim 65$ GeV. This is consistent with the exclusion from $\mathcal{B}^h_{\text{BSM}}$, as discussed below Eq. (24).

We now consider the resonance searches in the $\tau\tau$ channel at the LHC. Both ATLAS and CMS experiments presented their results based on the run-1 [65,66] and run-2 [67,68] data. Since the LHC run-1 data at $\sqrt{s} = 7 + 8$ TeV had weaker constraints, we focus on the run-2 results. In Fig. 8, we show $\sigma \times \mathcal{B}(A \rightarrow \tau\tau)$ in the 2HDM-SM4 at the 13-TeV LHC. As shown in the next subsection, the pseudoscalar A gets a much stronger constraint from the $\tau\tau$ channel than the CP-even H. This is partly because the gluon fusion production of A is more efficient due to a larger loop function than that of H (see Fig. 7). Another reason for this is the larger branching ratio of $A \rightarrow \tau\tau$ because of the absence of $A \rightarrow WW/ZZ/hh$. Both ATLAS and CMS experiments exclude the parameter space with $t_\beta \geq 4$ and $M_A \leq 2M_{b'}$. When $t_\beta = 3$ (the minimum value of t_β allowed by the observed κ_V), two experiments yield different lower bounds on M_A. Upon the absence of a combined ATLAS and CMS analysis, we take a conservative stance on constraining the model, i.e., adopting the weaker constraint between two experiment results. For $t_\beta = 3$, $M_A \lesssim 350$ GeV is excluded at the 95% C.L.

The smoking-gun signature for A at the LHC is the Zh channel, followed by $Z \rightarrow \ell\ell$ and $h \rightarrow b\bar{b}/\tau\tau$ [74–76]. In the SM, $pp \rightarrow Zh$ proceeds mainly through $q\bar{q} \rightarrow Zh$, mediated by Z^*. The gluon fusion production also occurs in the SM through the quark triangle diagram and the quark box diagram, Figs. 9(a) and 9(c). In the SM, $\sigma(gg \rightarrow Zh)$ is small, about 10% of the $q\bar{q}$ annihilation process, mainly because of the *destructive* interference between the triangle and box diagrams [77]. In the 2HDM-SM4, there are four kinds of new contributions: (i) $\sigma(q\bar{q} \rightarrow Zh)$ is reduced by a factor of κ_V^2; (ii) $\mathcal{B}(h \rightarrow b\bar{b}/\tau\tau)$ in the exact wrong-sign

TABLE I. Summary of the direct searches that are efficient for H/A in the 2HDM-SM4 at high energy colliders.

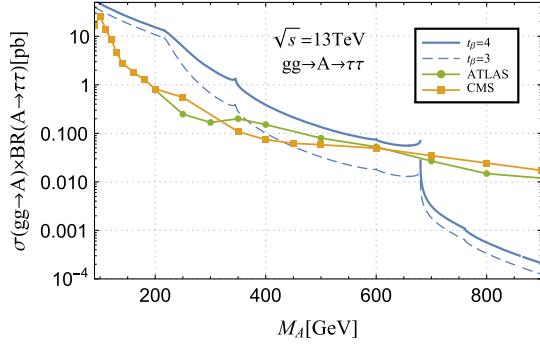| Process	Target	Mass range	Experiment
$e^+e^- \rightarrow 4b$, 4τ, $b\bar{b}\tau\tau$	A	$[2m_\tau, 100 \text{ GeV}]$	LEP [64]
$pp \rightarrow \tau\tau$	H, A	$[100 \text{ GeV}, 1 \text{ TeV}]$	LHC run 1 [65,66]
		$[90 \text{ GeV}, 3.2 \text{ TeV}]$	LHC run 2 [67,68]
$pp \rightarrow ZZ^{(*)}$	H	$[110 \text{ GeV}, 1 \text{ TeV}]$	LHC run 2 [69–72]
$pp \rightarrow Zh$	A	$[200, 1000]$	LHC run 1 [73,74]

FIG. 8.   We show $\sigma(gg \to A) \times \mathcal{B}(A \to \tau\tau)$ as a function of M_A at the 13-TeV LHC for $t_\beta = 3$ and $t_\beta = 4$. We apply the NNLO K factor to the heavy Higgs resonance production by using the HIGLU package [57]. For comparison, we also show the 95% C.L. upper limits on $\sigma \times \mathcal{B}(\phi \to \tau\tau)$ data [67,68].
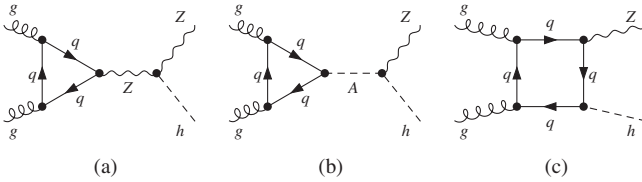

FIG. 9.   Feynman diagrams for the $gg \to Zh$ process in the 2HDM-SM4. Here q denotes all of the four generation quarks, including t' and b'.

limit is increased because of smaller $\Gamma(h \to WW/ZZ)$ than in the SM but the same $\Gamma(h \to b\bar{b}/\tau\tau)$; (iii) the fourth generation quarks contribute to all of the loop diagrams for $gg \to Zh$; (iv) new triangle diagrams mediated by A appear. In what follows, we call Fig. 9(a) the Z-triangle diagram, Fig. 9(b) the A-triangle diagram, and Fig. 9(c) the box diagram.

In order to see the interference effects in detail, we split the scattering amplitude into the Z-triangle part ($\mathcal{M}_Z$), the A-triangle part ($\mathcal{M}_A$), and the box part ($\mathcal{M}_\square$). The parton-level cross section becomes

$$\hat{\sigma} = \frac{1}{32\pi\hat{s}} \int d\cos\theta^* \overline{\sum} [|\mathcal{M}_Z|^2 + |\mathcal{M}_A|^2 + |\mathcal{M}_\square|^2$$
$$+ 2\Re e(\mathcal{M}_Z\mathcal{M}_A^*) + 2\Re e(\mathcal{M}_Z\mathcal{M}_\square^*) + 2\Re e(\mathcal{M}_A\mathcal{M}_\square^*)]$$
$$\equiv \hat{\sigma}_Z + \hat{\sigma}_A + \hat{\sigma}_\square + \hat{\sigma}_{ZA} + \hat{\sigma}_{Z\square} + \hat{\sigma}_{A\square}, \quad (30)$$

where θ^* is the scattering angle in the center-of-mass frame and $\overline{\sum}$ denotes the proper summation and average over helicities and colors. Figure 10 shows the individual contributions to the m_{Zh} distribution of the full $gg \to Zh$ for $t_\beta = 4$ and $M_A = 800$ GeV with $\Gamma_{\rm tot}^A = 2.0$ TeV at the 13-TeV LHC. We use $K_{q\bar{q}} = 1.31$ and $K_{gg} = 2.1$ to match up with the updated Higgs calculation results [78,79], and we assume the same K factor for the NP calculation. The cross section only from the Z-triangle diagrams, $d\sigma_Z$,
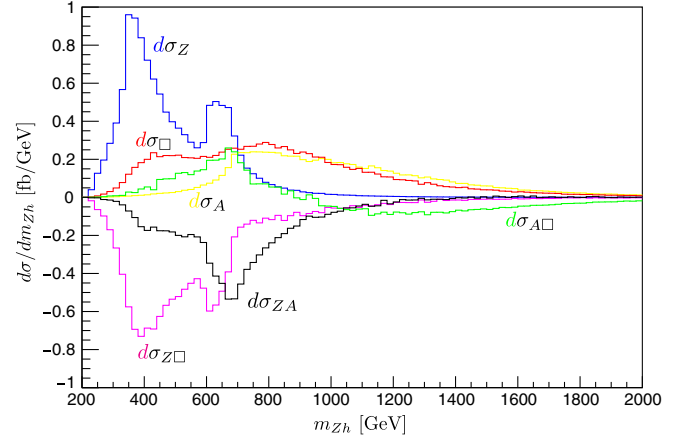

FIG. 10.   Invariant mass m_{Zh} distribution for $gg \to Zh$ production for $t_\beta = 4$ and $M_A = 800$ GeV at $\sqrt{s} = 13$ TeV. We plot individual contributions from the Z-triangle, A-triangle, box diagrams, and their interference terms. We use $K_{q\bar{q}} = 1.31$ and $K_{gg} = 2.1$ [78,79].

shows threshold behaviors around $m_{Zh} \simeq 2m_t$, $2M_{t'}$, $2M_{b'}$. The contribution from t' and b' is rather small because the corresponding transition amplitude is proportional to the axial vector coupling of the Z boson, $g_A^{Zff} = -(T_3^f)_L/2$ [79]. For almost degenerate masses of t' and b', two contributions are canceled. On the other hand, $d\sigma_\square$ has a large signal rate in the heavy m_{Zh} range because the opposite sign between $g_A^{Zb'b'}$ and $g_A^{Zt't'}$ is compensated by the opposite sign between $Y_{b'}^h$ and $Y_{t'}^h$. The $d\sigma_A/dm_{Zh}$ shows a very wide resonance shape, resulting in a small signal rate. Both $d\sigma_{Z\square}$ and $d\sigma_{ZA}$ yield destructive interference in the whole m_{Zh} region, large enough to almost cancel $d\sigma_Z$. The interference between the A-triangle and box diagrams is constructive for $m_{Zh} \leq M_A$, while it is destructive for $m_{Zh} \geq M_A$, a typical peak-dip structure [80]. In summary, the contributions from the interference are as large as noninterference ones.

In Fig. 11, we present the total invariant mass distribution in the SM and two 2HDM-SM4 cases: one with $t_\beta = 4$ and $M_A = 800$ GeV (pink line) and another with $t_\beta = 3$ and $M_A = 500$ GeV (blue line). We use $K_{q\bar{q}} = 1.31$ and $K_{gg} = 2.1$ [78,79]. For both NP cases, we calculate the full Feynman diagrams in Fig. 9. The total m_{Zh} distribution for $t_\beta = 4$ and $M_A = 800$ GeV, of which the individual contributions are shown in Fig. 10, shows a peculiar shape with two thresholds of $t\bar{t}$ and $b'\bar{b}'$ followed by a very slow downhill slope. This bizarre distribution is the consequence of large interference effects. The case with $t_\beta = 3$ and $M_H = 500$ GeV with $\Gamma_{\rm tot}^A = 13.8$ GeV yields a prominent peak over the SM main background of $q\bar{q} \to Zh$. The LHC experiments cannot miss the peak. Indeed, the total cross section of $pp \to Zh$ for $t_\beta = 3$ and $M_A = 500$ GeV is about 24.8 pb, far above the upper bound
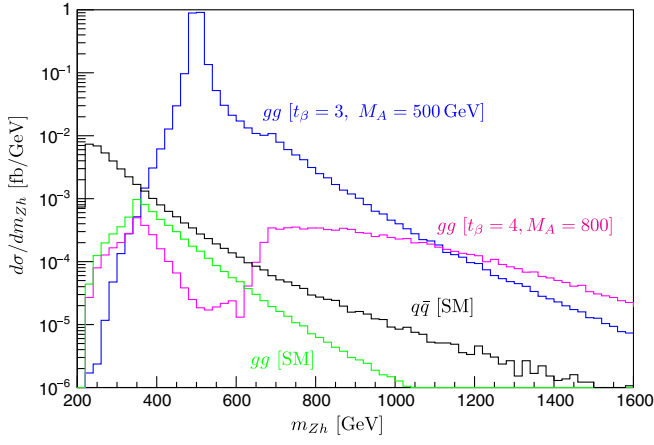
FIG. 11.   Invariant mass m_{Zh} distribution for the $pp \rightarrow Zh$ process at $\sqrt{s} = 13$ TeV. We separately present the $q\bar{q}$ contributions and the gg contributions in the SM and 2HDM-SM4. We consider two NP cases: (i) $t_\beta = 3$ and $M_A = 500$ GeV and (ii) $t_\beta = 4$ and $M_A = 800$ GeV in the benchmark scenario in Eq. (25). We use $K_{q\bar{q}} = 1.31$ and $K_{gg} = 2.1$ [78,79].

on $\sigma \times \mathcal{B}(A \rightarrow Zh) \simeq 0.854$ pb at $M_A = 500$ GeV. Larger t_β does not help to allow the model when $M_A \lesssim 2M_{b'}$: (i) The resonance peak becomes more prominent because of a smaller width for larger t_β in this mass range, as shown in Fig. 6; (ii) $t_\beta \gtrsim 4$ for $M_A < 2M_{b'}$ is already excluded by the $\tau\tau$ resonance searches as in Fig. 8. When $M_A \gtrsim 2M_{b'}$, the width becomes too wide to show a resonance peak. We calculate the partially integrated cross section for the excess in each m_{Zh} bin, defined in Eq. (28), and compare with the ATLAS result of the upper bounds on $\sigma \times \mathcal{B}(A \rightarrow Zh)$ [75]. We find that $t_\beta = 4$ and $M_A = 800$ GeV are still allowed. This conclusion is valid for larger t_β and $M_A > 2M_{b'}$.

B. Constraints from direct searches for H

For CP-even H, we first study the constraint from the resonance searches in the $\tau\tau$ channel based on the ATLAS and CMS run-2 data [67,68]. Figure 12 shows $\sigma \times \mathcal{B}(H \rightarrow \tau\tau)$ in the 2HDM-SM4 at the 13-TeV LHC. In the benchmark scenario, we consider two cases of $t_\beta = 3$ and $t_\beta = 4$. For the K factor, we take the NNLO result from the HIGLU package [57]. Compared with the rapid drop of $\mathcal{B}(H \rightarrow \tau\tau)$ as a function of M_H in Fig. 4, $\sigma \times \mathcal{B}(H \rightarrow \tau\tau)$ decreases slowly. This is because of the sizable cross section of the gluon fusion production of H for heavy M_H (see Fig. 7). The current LHC data in the $\tau\tau$ final states meaningfully exclude M_H, though less than the pseudoscalar A. Adopting the weaker constraint between two experiment results, $M_H < 180$ GeV ($M_H < 350$ GeV) is excluded for $t_\beta = 3$ ($t_\beta = 4$) at the 95% C.L.

The smoking-gun signature for the CP-even H is from the ZZ final state [69,70]. In the SM, the production of a Z boson pair is mainly through the $q\bar{q}$ annihilation. The gluon
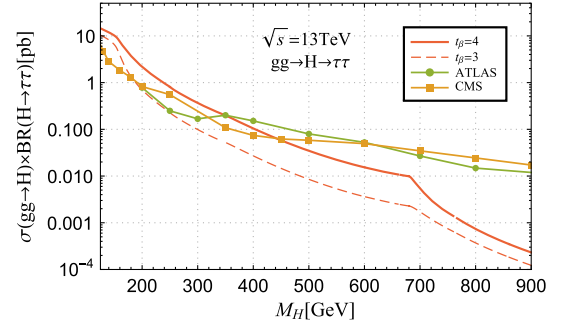

FIG. 12.   We show $\sigma(gg \rightarrow H) \times \mathcal{B}(H \rightarrow \tau\tau)$ as a function of M_H at the 13-TeV LHC. For two cases of $t_\beta = 3$ and $t_\beta = 4$, we set $M_{t'} = 300$ GeV, $M_{b'} = 340$ GeV, $M_{\nu'} = 430$ GeV, and $M_{\tau'} = 380$ GeV. We apply the NNLO K factor to the heavy Higgs resonance production by using the HIGLU package [57]. We also show the ATLAS and CMS 95% C.L. upper bounds on $\sigma \times \mathcal{B}(\phi \rightarrow \tau\tau)$.

fusion production via the quark loops is subleading, of which the cross section is about 10% of the Drell-Yan process. In the 2HDM-SM4, the Drell-Yan process $q\bar{q} \rightarrow ZZ$ is not affected since the CKM mixing V_{4i} is extremely suppressed. The gluon fusion process has three kinds of Feynman diagrams, as shown in Fig. 13: (a) the triangle diagrams mediated by h, (b) the triangle diagrams mediated by H, and (c) the box diagrams. New contributions are from the fourth generation quarks running in the loops and from the H-triangle diagram.

Figure 14 shows the noninterference contributions to $d\sigma/dm_{ZZ}(gg \rightarrow ZZ)$ from the h-triangle, H-triangle, and box diagrams as a function of m_{ZZ} at the 13-TeV LHC. We set $t_\beta = 4$ and $M_H = 900$ GeV and include $K_{gg} = 1.8$ and $K_{q\bar{q}} = 1.5$. The definition of $d\sigma_i$ is given in Eq. (30). The box diagrams ($d\sigma_\square$) yield the continuum background with a monotonically decreasing slope against m_{ZZ}, but the fourth generation quarks in the loop decrease the slope around the $b'\bar{b}'$ threshold. In terms of the total signal rate, the contribution from the box diagrams is dominant. The H-triangle diagrams yield a very wide resonance peak around $M_A = 900$ GeV. In the range of $m_{ZZ} \gtrsim 1$ TeV, the contribution from the H-triangle diagrams is as large as that from the box diagrams. On the other hand, the h-triangle diagrams make a negligible contribution in the whole range of m_{ZZ}. The total distribution denoted by the black line
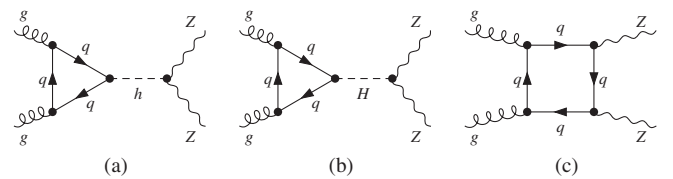

FIG. 13.   Feynman diagrams for the $gg \rightarrow ZZ$ process in the 2HDM-SM4. Here q denotes all of the four generation quarks, including t' and b'.
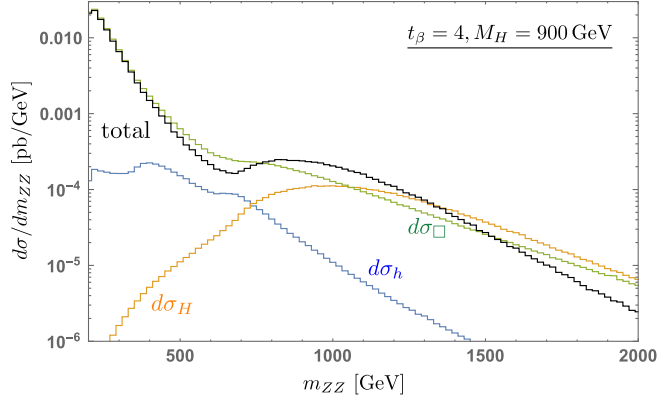
FIG. 14. The differential cross section for $gg \rightarrow ZZ$ against m_{ZZ} in the 2HDM-SM4 at the 13-TeV LHC. We set $t_\beta = 4$ and $M_H = 900$ GeV. We show individual contributions from the h-triangle, H-triangle, and box diagrams. We include $K_{gg} = 1.8$ [81] and $K_{q\bar{q}} = 1.5$ [82].

FIG. 16. The differential cross section against m_{ZZ} in the SM and 2HDM-SM4 at the 13-TeV LHC. We consider three NP cases: $t_\beta = 3$ and $M_H = 500$ GeV; $t_\beta = 4$ and $M_H = 900$ GeV; $t_\beta = 7$ and $M_H = 900$ GeV for the benchmark point. We include $K_{gg} = 1.8$ [81] and $K_{q\bar{q}} = 1.5$ [82].

shows some deviation from the simple sum of $d\sigma_\square + d\sigma_H + d\sigma_h$, especially around $m_{ZZ} \sim 700$ GeV. Obviously, the interference plays a role.

In Fig. 15, we show the three kinds of interference effects, $d\sigma_{ij}$ defined in Eq. (30), that are too small to show, together with noninterference $d\sigma_i$ in a single plot. First, the interference between the h-triangle and box diagrams, $\sigma_{h\square}$, is destructive and largest. We observe the threshold effects around $2m_t$ and $2M_{b'}$. The interference $d\sigma_{H\square}$ shows a very asymmetric and wide peak-dip structure [83], practically like a wide peak of constructive interference. The opposite sign between $d\sigma_{h\square}$ and $d\sigma_{H\square}$ is attributed to the opposite sign between the $hb'\bar{b}'$ and $Hb'\bar{b}'$ couplings. Finally, $d\sigma_{hH}$ is destructive but negligible.

Figure 16 shows the total invariant mass m_{ZZ} distributions of $q\bar{q} \rightarrow ZZ$ in the SM, and $gg \rightarrow ZZ$ in the SM and the 2HDM-SM4. We consider three NP cases: (i) $t_\beta = 3$ and $M_H = 500$ GeV, (ii) $t_\beta = 4$ and $M_H = 900$ GeV, and (iii) $t_\beta = 7$ and $M_H = 900$ GeV. It is clear to see that the
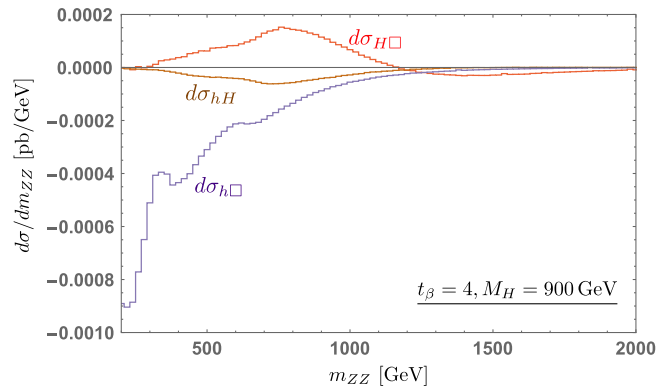
case of $t_\beta = 3$ and $M_H = 500$ GeV, which was allowed by the $\tau\tau$ constraint in Fig. 12, yields a very outstanding peak because of a relatively narrow width and large production rate of $gg \rightarrow H$. Apparently, the current upper bound on $\sigma \times \mathcal{B}(\phi \rightarrow ZZ)$ excludes this case. Note that the whole parameter space with $M_H < 2M_{b'}$ (where H remains as a prominent peak) is excluded since larger t_β yields a larger production cross section of $gg \rightarrow H$ as shown in Fig. 7.

When M_H is above the $b'\bar{b}'$ threshold, as shown by two cases of $t_\beta = 4, 7$ with $M_H = 900$ GeV, the very large width of H spreads the H resonance peak. It can be seen that the signal rate of $gg \rightarrow ZZ$ in the 2HDM-SM4 is compatible with the SM Drell-Yan production rate in the mass range of $m_{ZZ} \gtrsim 1$ TeV. Comparing the $t_\beta = 4$ ($\Gamma_{\text{tot}}^H = 1.3$ TeV) and $t_\beta = 7$ ($\Gamma_{\text{tot}}^H = 3.6$ TeV) cases, we find that the dependence on t_β is not dramatically different once M_H is beyond the $b'\bar{b}'$ threshold. In order to probe this very wide resonance, we adopt the method suggested at the end of Sec. VA, utilizing the 95% C.L. upper limits on $\sigma \times \mathcal{B}(H \rightarrow ZZ)$ for each invariant mass bin. Since the CMS Collaboration presented the results for $\Gamma_X = 100$ GeV, we take the CMS results [69].

In Fig. 17, we show the partially integrated cross section from NP effects only, $\Delta\sigma^{\text{NP}}$, for various m_{ZZ} bins. The sizes of the bins are based on the CMS results [69]. We set $M_H = 900$ GeV and consider two cases of $t_\beta = 4$ and $t_\beta = 7$. The red region is excluded by the 95% C.L. upper bounds on $\sigma \times \mathcal{B}(H \rightarrow ZZ)$. Both $t_\beta = 4$ and $t_\beta = 7$ cases are excluded by the bin of $m_{ZZ} \in [1, 1.5]$ TeV. Larger t_β, apart from the breakdown of the perturbativity of $Y_{b'}^H$, does not help us to decrease the signal rate of NP since the gluon fusion production cross section increases with larger t_β. Note that we cannot increase M_H substantially further since $M_H = 900$ GeV is almost a maximally allowed value by the theoretical constraint (see Fig. 1). In summary, the

FIG. 15. The differential cross section for $gg \rightarrow ZZ$ against m_{ZZ} from the interference terms. We set $t_\beta = 4$ and $M_H = 900$ GeV at the 13-TeV LHC. We include $K_{gg} = 1.8$ [81] and $K_{q\bar{q}} = 1.5$ [82].
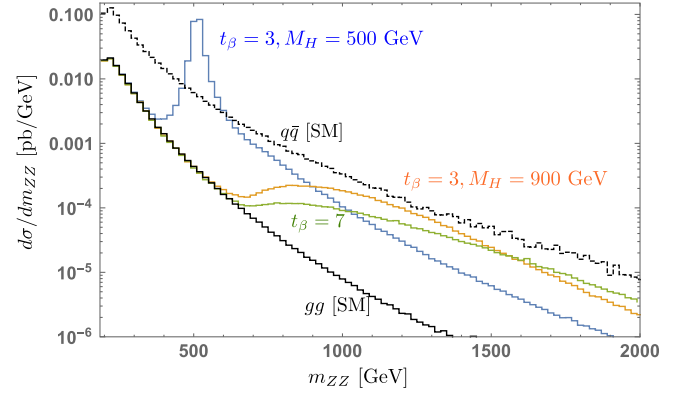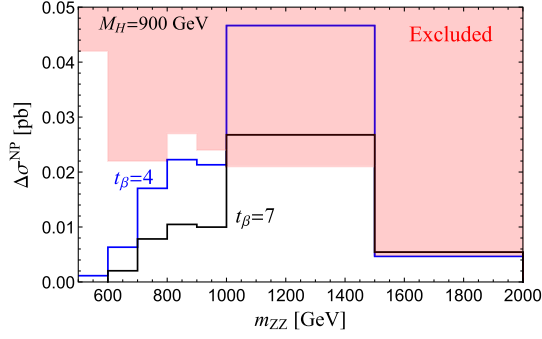
FIG. 17. Partially integrated cross section of NP effects only, $\Delta\sigma^{\rm NP}$ defined in Eq. (28), for various m_{ZZ} bins. We set $M_H = 900$ GeV and consider $t_\beta = 4$ and $t_\beta = 7$. The red region is excluded by the 95% C.L. upper bounds on $\sigma \times \mathcal{B}(H \to ZZ)$.

current LHC data on the ZZ channel, along with theoretical constraints, exclude the 2HDM-SM4 at leading order.

VII. CONCLUSIONS

We have studied the theoretical and phenomenological constraints on the type-II two-Higgs-doublet model with a sequential fourth fermion generation in the exact wrong-sign limit, the 2HDM-SM4. The SM fermion sector is extended to accommodate an additional chiral fermion generation of which the masses are generated by the same Higgs mechanism. Upon the absence of new fermion signals at high energy colliders, the fourth generation fermion F should be heavy, which greatly enhances the hFF couplings. The loop-induced Higgs coupling modifiers such as κ_g, κ_γ, and $\kappa_{Z\gamma}$ become SM-like if the up-type and down-type fermions have opposite Higgs coupling modifiers: $\kappa_{\rm up} = 1$ and $\kappa_{\rm down} = -1$. We call this the exact wrong-sign limit, which can be realized in the type-II 2HDM.

We have studied the following constraints: (i) the theoretical constraints on the scalar potential from the bounded-from-below potential, unitarity, perturbativity, and the vacuum stability; (ii) the LHC and Tevatron search bounds on the fourth generation fermion masses; (iii) the $\bar{B} \to X_s\gamma$ bound on $M_{H^\pm}$; (iv) the electroweak oblique parameters ΔS and ΔT; (v) the observed Higgs coupling modifiers, including the exotic Higgs decay rate; (vi) the LEP searches for $e^+e^- \to Ah$; and (vii) the LHC scalar resonance searches in the $\tau\tau$, Zh, and ZZ modes. Based on this comprehensive and thorough study, we come to the conclusion that the 2HDM-SM4 is excluded at leading order. Two features of the 2HDM-SM4 play a crucial role here: the exact wrong-sign limit and the very large Yukawa couplings of the down-type fourth generation fermions with H and A, $Y_{b',\tau'}^{H/A} = \tan\beta M_F/v$.

The exact wrong-sign limit requiring $\beta + \alpha = \pi/2$ constrains the model very differently than the alignment limit of $\beta - \alpha = \pi/2$. First, the theoretical constraints do not allow the decoupling limit, which puts *upper* bounds like

M_H, $M_A \lesssim 920$ GeV and $M_{H^\pm} \lesssim 620$ GeV. Second, the constraint on $\tan\beta$ from the Higgs precision data works in the opposite way compared to that from the unitarity of $Y_{b',\tau'}^{H/A} = \tan\beta M_F/v$. The observed $\kappa_V (= s_{\beta-\alpha})$ at 95% C.L. requires $\tan\beta \gtrsim 3$, while the unitarity of $Y_{b',\tau'}^{H/A}$ requires $\tan\beta \lesssim 8$. The allowed value of $\tan\beta \in [3,8]$ is not large enough to achieve the alignment limit: $\kappa_V (= s_{\beta-\alpha})$ deviates significantly from 1 and thus $c_{\beta-\alpha}$ has a sizable value. Therefore, the usual 2HDM safety zone in the alignment and decoupling limit cannot be reached in the 2HDM-SM4.

These indirect constraints set the basic characteristics of the decays of H and A. Two features are to be noted. First, the sizable $c_{\beta-\alpha}$ leads to significant decays of $H \to WW/ZZ/hh$ and $A \to Zh$, which would have been absent in the alignment limit. Above the WW/ZZ (Zh) and below the $b'\bar{b}'$ threshold, H (A) decays dominantly into $WW/ZZ/hh$ (Zh). After the $b'\bar{b}'$ threshold, the enhanced Yukawa coupling $Y_{b'}^{H/A}$ makes the decay of $H/A \to b'\bar{b}'$ dominant. Because of the sizable $\Gamma(H/A \to gg)$ and non-negligible $\mathcal{B}(H/A \to \tau\tau)$, the LHC direct searches in the $\tau\tau$ channel impose the strong constraint: For $t_\beta = 4$, $M_A < 2M_{b'}$ and $M_H < 350$ GeV are excluded; for $t_\beta = 3$, $M_A \lesssim 350$ GeV and $M_H < 180$ GeV are excluded at the 95% C.L.

The smoking-gun signatures of A and H are the LHC direct searches in the Zh and ZZ channels, respectively. Since their total decay widths are not small enough to adopt the narrow-width approximation, we performed the full calculation including the SM continuum background without resorting to $\sigma \times \mathcal{B}$. The interference effects turned out to be very important. In the $gg \to Zh$ process, they are as much as the noninterference ones. We found that both A and H with the mass below the $b'\bar{b}'$ threshold are excluded by the current LHC data at the 95% C.L. Above the $b'\bar{b}'$ threshold, $\Gamma_{\rm tot}^{H/A}$ becomes very large and is compatible with the mass $M_{H/A}$. The invariant mass distributions spread very widely. Beyond relying on the total event rates, we suggested a method to utilize the upper bounds on $\sigma \times \mathcal{B}$ on each invariant mass bin, through the partially integrated cross section. Although the pseudoscalar A with $M_A > 2M_{b'}$ is allowed by the current LHC data in the Zh channel, the CP-even heavy scalar H is excluded by the current LHC data in the ZZ channel.

We conclude that the 2HDM-SM4 is excluded by the combination of the theoretical and experimental constraints at leading order. Before finishing, however, we would like to point out two issues. First, we assumed nearly degenerate heavy scalar masses as well as degenerate fourth generation fermion masses for the oblique ΔT parameter. Sizable mass differences are still possible if the contribution from heavy scalars to ΔT is canceled by that from the fourth generation fermions. However, we found that the upper bound on M_H, which played a crucial role in excluding the model, is not changed much by relaxing the degenerate condition: The

conclusion remains the same. A more crucial limitation of our conclusion is that our results are based on leading-order calculations. The conclusion may be relaxed if we consider the next-to-leading order corrections. The sizable $\cos(\beta - \alpha)$, the multiplying factor for the HVV and AZh couplings at tree level, plays a decisive role in excluding the model. With the fourth generation fermions running in the loop, both HVV and AZh couplings can be meaningfully different from the tree-level results. The constraints from the LHC resonance searches in the ZZ and Zh final states may be alleviated.

[1] P. H. Frampton, P. Q. Hung, and M. Sher, Phys. Rep. **330,** 263 (2000).

[2] D. Choudhury, T. M. P. Tait, and C. E. M. Wagner, Phys. Rev. D **65,** 053002 (2002).

[3] M. Bobrowski, A. Lenz, J. Riedl, and J. Rohrwild, Phys. Rev. D **79,** 113006 (2009).

[4] G. Aad *et al.* (ATLAS Collaboration), Phys. Lett. B **716,** 1 (2012).

[5] S. Chatrchyan *et al.* (CMS Collaboration), Phys. Lett. B **716,** 30 (2012).

[6] D. Das, A. Kundu, and I. Saha, Phys. Rev. D **97,** 011701 (2018).

[7] G. Bhattacharyya, D. Das, and P. B. Pal, Phys. Rev. D **87,** 011702 (2013).

[8] D. Carmi, A. Falkowski, E. Kuflik, and T. Volansky, J. High Energy Phys. 07 (2012) 136.

[9] C. W. Chiang and K. Yagyu, J. High Energy Phys. 07 (2013) 160.

[10] P. M. Ferreira, J. F. Gunion, H. E. Haber, and R. Santos, Phys. Rev. D **89,** 115003 (2014).

[11] D. Fontes, J. C. Romo, and J. P. Silva, Phys. Rev. D **90,** 015021 (2014).

[12] N. Chen and H. J. He, J. High Energy Phys. 04 (2012) 062.

[13] A. I. Hernndez-Jurez, A. Moyotl, and G. Tavares-Velasco, Phys. Rev. D **98,** 035040 (2018).

[14] L. Wang, R. Shi, and X. F. Han, Phys. Rev. D **96,** 115025 (2017).

[15] S. Chamorro-Solano, A. Moyotl, and M. A. Prez, J. Phys. G **45,** 075003 (2018).

[16] G. C. Branco, P. M. Ferreira, L. Lavoura, M. N. Rebelo, M. Sher, and J. P. Silva, Phys. Rep. **516,** 1 (2012).

[17] S. L. Adler, Phys. Rev. **177,** 2426 (1969).

[18] J. S. Bell and R. Jackiw, Nuovo Cimento A **60,** 47 (1969).

[19] S. L. Glashow and S. Weinberg, Phys. Rev. D **15,** 1958 (1977).

[20] E. A. Paschos, Phys. Rev. D **15,** 1966 (1977).

[21] M. D. Campos, D. Cogollo, M. Lindner, T. Melo, F. S. Queiroz, and W. Rodejohann, J. High Energy Phys. 08 (2017) 092.

[22] S. Chang, S. K. Kang, J. P. Lee, and J. Song, Phys. Rev. D **92,** 075023 (2015).

[23] J. Bernon, J. F. Gunion, H. E. Haber, Y. Jiang, and S. Kraml, Phys. Rev. D **93,** 035027 (2016).

[24] J. F. Gunion and H. E. Haber, Phys. Rev. D **67,** 075019 (2003).

[25] A. Djouadi, Phys. Rep. **457,** 1 (2008).

[26] P. M. Ferreira, R. Guedes, M. O. P. Sampaio, and R. Santos, J. High Energy Phys. 12 (2014) 067.

[27] I. F. Ginzburg and M. Krawczyk, Phys. Rev. D **72,** 115013 (2005).

[28] A. Dighe, D. Ghosh, R. M. Godbole, and A. Prasath, Phys. Rev. D **85,** 114035 (2012).

[29] S. Dawson and P. Jaiswal, Phys. Rev. D **82,** 073017 (2010).

[30] S. Chatrchyan *et al.* (CMS Collaboration), Phys. Rev. D **86,** 112003 (2012).

[31] A. Lister (CDF Collaboration), arXiv:0810.3349.

[32] T. Aaltonen *et al.* (CDF Collaboration), Phys. Rev. Lett. **104,** 091801 (2010).

[33] C. J. Flacco, D. Whiteson, T. M. P. Tait, and S. Bar-Shalom, Phys. Rev. Lett. **105,** 111801 (2010).

[34] C. J. Flacco, D. Whiteson, and M. Kelly, Phys. Rev. D **83,** 114048 (2011).

[35] C. Patrignani *et al.* (Particle Data Group), Chin. Phys. C **40,** 100001 (2016).

[36] M. Misiak and M. Steinhauser, Eur. Phys. J. C **77,** 201 (2017).

[37] M. Misiak, Acta Phys. Pol. B **48,** 2173 (2017).

[38] A. Abdesselam *et al.* (Belle Collaboration), arXiv:1608.02344.

[39] P. M. Ferreira, R. Guedes, J. F. Gunion, H. E. Haber, M. O. P. Sampaio, and R. Santos, arXiv:1407.4396.

[40] I. P. Ivanov, Phys. Rev. D **75,** 035001 (2007); **76,** 039902(E) (2007).

[41] B. W. Lee, C. Quigg, and H. B. Thacker, Phys. Rev. D **16,** 1519 (1977).

[42] S. Kanemura and K. Yagyu, Phys. Lett. B **751,** 289 (2015).

[43] A. Arhrib, arXiv:hep-ph/0012353.

[44] A. Barroso, P. M. Ferreira, I. P. Ivanov, and R. Santos, J. High Energy Phys. 06 (2013) 045.

[45] G. D. Kribs, T. Plehn, M. Spannowsky, and T. M. P. Tait, Phys. Rev. D **76,** 075016 (2007).

[46] W. Grimus, L. Lavoura, O. M. Ogreid, and P. Osland, J. Phys. G **35,** 075001 (2008).

[47] W. Grimus, L. Lavoura, O. M. Ogreid, and P. Osland, Nucl. Phys. **B801,** 81 (2008).

[48] G. Aad et al. (ATLAS and CMS Collaborations), J. High Energy Phys. 08 (2016) 045.

[49] M. Aaboud et al. (ATLAS Collaboration), J. High Energy Phys. 03 (2018) 095.

[50] A. M. Sirunyan et al. (CMS Collaboration), J. High Energy Phys. 11 (2017) 047.

[51] Y. W. Yoon, K. Cheung, S. K. Kang, and J. Song, Phys. Rev. D **96,** 055041 (2017).

[52] M. Aaboud et al. (ATLAS Collaboration), Phys. Rev. D **98,** 052005 (2018).

[53] CMS Collaboration, CERN, Report No. CMS-PAS-HIG-16-040, 2017.

[54] S. Chatrchyan et al. (CMS Collaboration), Phys. Rev. D **89,** 092007 (2014).

[55] M. Aaboud et al. (ATLAS Collaboration), Phys. Rev. D **96,** 052004 (2017).

[56] R. Franceschini, G. F. Giudice, J. F. Kamenik, M. McCullough, A. Pomarol, R. Rattazzi, M. Redi, F. Riva, A. Strumia, and R. Torre, J. High Energy Phys. 03 (2016) 144.

[57] M. Spira, arXiv:hep-ph/9510347.

[58] A. Djouadi, Phys. Rep. **459,** 1 (2008).

[59] D. J. Miller, S. Moretti, D. P. Roy, and W. J. Stirling, Phys. Rev. D **61,** 055011 (2000).

[60] G. Aad et al. (ATLAS Collaboration), Phys. Rev. Lett. **113,** 171801 (2014).

[61] CMS Collaboration, CERN, Report No. CMS-PAS-HIG-17-013, 2017.

[62] G. Aad et al. (ATLAS Collaboration), Phys. Lett. B **759,** 601 (2016).

[63] M. Aaboud et al. (ATLAS Collaboration), Phys. Rev. D **98,** 032016 (2018).

[64] S. Schael et al. (ALEPH, DELPHI, L3, and OPAL Collaborations, LEP Working Group for Higgs Boson Searches), Eur. Phys. J. C **47,** 547 (2006).

[65] G. Aad et al. (ATLAS Collaboration), J. High Energy Phys. 11 (2014) 056.

[66] V. Khachatryan et al. (CMS Collaboration), J. High Energy Phys. 10 (2014) 160.

[67] M. Aaboud et al. (ATLAS Collaboration), J. High Energy Phys. 01 (2018) 055.

[68] A. M. Sirunyan et al. (CMS Collaboration), J. High Energy Phys. 09 (2018) 007.

[69] A. M. Sirunyan et al. (CMS Collaboration), J. High Energy Phys. 06 (2018) 127.

[70] M. Aaboud et al. (ATLAS Collaboration), J. High Energy Phys. 03 (2018) 009.

[71] V. Khachatryan et al. (CMS Collaboration), J. High Energy Phys. 10 (2015) 144.

[72] G. Aad et al. (ATLAS Collaboration), Eur. Phys. J. C **76,** 45 (2016).

[73] V. Khachatryan et al. (CMS Collaboration), Phys. Lett. B **748,** 221 (2015).

[74] G. Aad et al. (ATLAS Collaboration), Phys. Lett. B **744,** 163 (2015).

[75] ATLAS Collaboration, CERN, Report No. ATLAS-CONF-2016-015, 2016.

[76] CMS Collaboration, CERN, Report No. CMS-PAS-HIG-18-005, 2018.

[77] C. Englert, M. McCullough, and M. Spannowsky, Phys. Rev. D **89,** 013013 (2014).

[78] D. de Florian et al. (LHC Higgs Cross Section Working Group), Handbook of LHC Higgs Cross Sections: 4. Deciphering the Nature of the Higgs Sector, CERN Yellow Reports: Monographs, Vol. 2 (CERN, Geneva, Switzerland, 2017).

[79] L. M. Carpenter, T. Han, K. Hendricks, Z. Qian, and N. Zhou, Phys. Rev. D **95,** 053003 (2017).

[80] S. Jung, Y. W. Yoon, and J. Song, Phys. Rev. D **93,** 055035 (2016).

[81] F. Caola, K. Melnikov, R. Röntsch, and L. Tancredi, Phys. Rev. D **92,** 094028 (2015).

[82] F. Cascioli, T. Gehrmann, M. Grazzini, S. Kallweit, P. Maierhöfer, A. von Manteuffel, S. Pozzorini, D. Rathlev, L. Tancredi, and E. Weihs, Phys. Lett. B **735,** 311 (2014).

[83] S. Jung, J. Song, and Y. W. Yoon, Phys. Rev. D **92,** 055009 (2015).